

Suppression of electron thermal conduction in the high β intracluster medium of galaxy clusters

G. T. Roberg-Clark¹, J. F. Drake^{2,5,6,7}, C. S. Reynolds^{3,7}, M. Swisdak^{4,6,7}

ABSTRACT

Understanding the thermodynamic state of the hot intracluster medium (ICM) in a galaxy cluster requires a knowledge of the plasma transport processes, especially thermal conduction. The basic physics of thermal conduction in plasmas with ICM-like conditions has yet to be elucidated, however. We use particle-in-cell simulations and analytic models to explore the dynamics of an ICM-like plasma (with small gyroradius, large mean-free-path, and strongly sub-dominant magnetic pressure) induced by the diffusive heat flux associated with thermal conduction. Linear theory reveals that whistler waves are driven unstable electron heat flux, even when the heat flux is weak. The resonant interaction of electrons with these waves then plays a critical role in scattering electrons and suppressing the heat flux. In a 1D model where only whistler modes that are parallel to the magnetic field are captured, the only resonant electrons are moving in the opposite direction to the heat flux and the electron heat flux suppression is small. In 2D or more, oblique whistler modes also resonate with electrons moving in the direction of the heat flux. The overlap of resonances leads to effective symmetrization of the electron distribution function and a strong suppression of heat flux. The results suggest that thermal conduction in the ICM might be strongly suppressed, possibly to negligible levels.

¹Department of Physics, University of Maryland, College Park, MD 20742, USA; grc@umd.edu

²Department of Physics, University of Maryland, College Park, MD 20742, USA; drake@umd.edu

³Department of Astronomy, University of Maryland, College Park, MD 20742, USA; chris@astro.umd.edu

⁴Department of Physics, University of Maryland, College Park, MD 20742, USA; swisdak@umd.edu

⁵Institute for Physical Science and Technology, University of Maryland, College Park, MD 20742, USA

⁶Institute for Research in Electronics and Applied Physics, University of Maryland, College Park, MD 20742, USA

⁷Joint Space-Science Institute (JSI), College Park, MD 20742, USA

Subject headings: conduction — galaxies: clusters: intracluster medium — methods: numerical — plasmas — turbulence

1. Introduction

Over 80% of the baryonic matter in a galaxy cluster resides in an atmosphere of hot plasma, the intracluster medium (ICM), which is in a state of approximate hydrostatic equilibrium within the gravitational potential of the cluster’s dark matter halo. In many clusters, X-ray measurements of the electron number density ($n_e \sim 10^{-3} - 10^{-1} \text{ cm}^{-3}$) and temperature ($T \sim 10^7 - 10^8 \text{ K}$) reveal ICM cores that have short cooling times ($t_{\text{cool}} < 10^9 \text{ yr}$) and depressed temperatures (Fabian 1994). If unchecked, the radiative losses in these cool-core clusters would lead to significant accumulations of cold gas within the central galaxy, resulting in star formation rates of $100 - 1000 \text{ M}_{\odot} \text{ yr}^{-1}$, and central galaxies with stellar masses of $10^{13} \text{ M}_{\odot}$ or more (Croton et al. 2006). Observed star formation rates and total stellar masses in these systems are an order of magnitude smaller, demonstrating that the radiative losses of the ICM must be largely offset. The current paradigm is that energy injection by a central jetted active galactic nucleus (AGN) is thermalized in the ICM (Churazov et al. 2000, 2002; Reynolds et al. 2002). Thermal conduction within the ICM is very likely to play a central role in these astrophysical processes by dissipating weak shocks and sound waves driven by the AGN, and strongly modifying local thermal instabilities (Binney & Cowie 1981; Fabian et al. 2005; Yang & Reynolds 2016, and references therein). The direct transport of heat from the outer (hotter) regions of the ICM may also be a source of heat for the ICM cool-core.

Thermal conduction in the ICM plasma remains poorly understood. At these densities and temperatures, the electron mean free path is $\lambda \sim 0.1 - 1 \text{ kpc}$. With measured magnetic fields of $B \sim 1 - 10 \mu\text{G}$, the electron gyro-radius $\rho_e \sim 10^8 \text{ cm}$ is many orders of magnitude smaller so transport is highly anisotropic. Most current treatments of the ICM adopt a fluid description, taking the thermal conductivity to have the canonical Spitzer value (Spitzer 1956) along the local magnetic field and complete suppression in the orthogonal direction. However, Spitzer conductivity is not likely to be valid in the low collisionality ICM plasma where collisional mean-free-paths and temperature scale lengths can be comparable. Furthermore, the fact that the ratio of thermal-to-magnetic pressure is large, $\beta \equiv 8\pi nT/B^2 \sim 100$ suggests that the ICM is susceptible to instabilities driven by pressure anisotropies and heat fluxes that are expected to impede thermal conduction (Gary & Li 2000; Li et al. 2012; Kunz et al. 2014; Rincon et al. 2015).

In this paper we explore how self-generated turbulence impacts the thermal conductivity of a high- β ICM plasma. Unlike in earlier models in which the pressure anisotropy in the high- β medium is a source of turbulence that impacts thermal conduction (Riquelme et al. 2016; Komarov et al. 2016), we focus directly on the electron heat flux as a source of free energy. We show that whistler waves driven by the heat flux are generically unstable in the ICM. Particle-in-cell (PIC) simulations of the turbulence reveal strong heat-flux suppression. A comparison of the results of 1D and 2D simulations with an analytic model reveals the importance of the resonant interaction between the electrons and waves and associated particle trapping in facilitating strong scattering.

2. 1D Instability Model

We solve the linearized Vlasov-Maxwell equations to obtain a dispersion relation for whistler-like modes propagating along the local magnetic field $\mathbf{B} = B_0 \hat{\mathbf{x}}$. The temperature T is taken to be uniform but we include a heat flux as a source of free energy. We neglect ion contributions, which scale like $\sqrt{m_e/m_i}$ and are small in simulations (not shown). Making the standard whistler assumptions, we obtain the dispersion relation for the frequency ω of modes with wave vector k along \mathbf{B} , (Krall & Trivelpiece 1986):

$$\frac{k^2 c^2}{\omega^2} - \frac{\omega_{pe}^2}{\omega n_0} \int d^3 \mathbf{v} \frac{v_{\perp}}{2} \frac{\left[\left(1 - \frac{kv_x}{\omega}\right) \frac{\partial f_0}{\partial v_{\perp}} + \frac{kv_{\perp}}{\omega} \frac{\partial f_0}{\partial v_x} \right]}{\omega - kv_x - \Omega_e} = 0 \quad (1)$$

where $\omega_{pe} = (4\pi n_0 e^2/m_e)^{1/2}$ is the plasma frequency, $\Omega_e = eB_0/m_e c$ is the cyclotron frequency, $f_0(\mathbf{v})$ is the initial electron phase space distribution, $v_{Te} = (2T_e/m_e)^{1/2}$ is the thermal speed, $\rho_e = v_{Te}/\Omega_e$ is the Larmor radius, $d_e = c/\omega_{pe}$ the skin depth and $\beta_e = 8\pi n_0 T_e/B^2$.

In the standard whistler ordering with $\omega \sim (kd_e)^2 \Omega_e \sim \Omega_e$ and $kd_e \sim 1$, waves in high beta plasmas resonate with bulk electrons, $v_x \sim \Omega_e/k \sim \Omega_e d_e \sim v_{Te}/\sqrt{\beta_e} \ll 1$, and are therefore heavily damped. Thus whistlers with conventional ordering do not exist in high beta plasmas. To obtain wave growth we consider longer wavelength modes with $\omega \sim (kd_e)^2 \Omega_e \ll \Omega_e$. Resonant particles have $v_x \sim \Omega_e/k \sim v_{Te}/(k\rho_e)$. Requiring $v_x \gtrsim v_{Te}$ yields $k\rho_e \lesssim 1$ with $\omega \sim \Omega_e/\beta_e \ll \Omega_e$.

To model heat flux instability we use a distribution function from Levinson & Eichler (1992)

$$f_0(\mathbf{v}) = f_m \left[1 + \epsilon \left(\frac{v^2}{v_{Te}^2} - \frac{5}{2} \right) \frac{v_x}{v_{Te}} \right] \quad (2)$$

where $f_m = n_{0e}/(\sqrt{\pi}v_{Te})^3 \exp[-v^2/v_{Te}^2]$ and the term proportional to $\epsilon = v_{Te}/(\nu_{ei}L_T) \ll 1$ yields a heat flux (see also Ramani & Laval (1978)). Equation 2 was obtained by balancing a large-scale temperature gradient (along \mathbf{B}_0) $\partial T/\partial x \equiv T/L_T$ with a Krook collision operator. f_0 has no net drift ($\langle \mathbf{v} \rangle = 0$) and the plasma pressure is isotropic. The sole driver for instability is the heat flux, $q_{x0} = mn_0\langle v_x v^2 \rangle/2 = (5/8)\epsilon mn_0 v_{Te}^3$. Using this distribution function and taking $\omega \ll \Omega_e$ in Eq. 1 the frequency becomes

$$\omega = \frac{\Omega_e}{\beta_e} (k^2 \rho_e^2 + \epsilon \beta_e k \rho_e h_2) \frac{1}{h_1}, \quad (3)$$

where

$$h_1(k\rho_e, \epsilon) = \frac{\Omega_e}{kn_0} \int d^3\mathbf{v} \frac{f_0}{v_x + \Omega_e/k}$$

and

$$h_2(k\rho_e) = \frac{1}{k\rho_e} \frac{1}{\epsilon} \int d^3\mathbf{v} \frac{v_x f_0 + (v_{\perp}^2/2)\partial f_0/\partial v_x}{v_x + \Omega_e/k}.$$

h_2 is only non-zero because of the heat flux and the integral over v_x must go under the singularity at $v_x = -\Omega_e/k \equiv v_r$, the parallel resonant velocity. The real frequency ω_r and growth rate γ versus k for $\beta_e = 32, 100$ and $\epsilon = 0.133$ are presented in Fig. 1(a). The growth rate γ is peaked around $k\rho_e \sim 1$ and goes to zero for small and large $k\rho_e$. The waves have whistler-like dispersion for small k but the frequency rolls over at $k\rho_e \simeq 0.6$ and has a characteristic phase speed $v_{ph} = \omega/k \sim \rho_e \Omega_e/\beta_e = v_{Te}/\beta_e \ll v_{Te}$. The resonant interaction is with particles with $v_x \sim -v_r \sim -v_{te}$. In Fig. 1b the maximum growth rate (with respect to k) is plotted against $\beta\epsilon$. Instability exists for any non-zero value of ϵ so there is no threshold for the instability. This is highly relevant to the ICM, for which $\epsilon \ll 1$ (Levinson & Eichler 1992). We now present numerical simulations to verify (3) and to probe the impact on the heat flux.

3. Numerical Methods

We simulate the instability using the particle-in-cell (PIC) code `p3d` (Zeiler et al. 2002). Particle trajectories are calculated using the relativistic Newton-Lorentz equations and the electromagnetic fields are advanced using Maxwell's equations. We present the results of quasi-1D, collisionless simulations (3600 particles per cell) with dimensions $L_x \times L_y = 28.96\rho_e \times 1.80\rho_e$ (a finite L_y increases the number of particles and reduces particle noise) and a 2D simulation with $L_x \times L_y = 28.96\rho_e \times 28.96\rho_e$ (800 particles per cell). Periodic boundary conditions are used in both x and y with $\beta_{e0} = 32$. With these values

of L_x and L_y many unstable modes of scale ρ_e can fit in the box. Ions form a stationary, charge-neutralizing background.

There is no ambient temperature gradient but we initialize electrons with the distribution given in Eq. 2. Since f_0 is not strictly positive we adjust our initial distribution to ensure that $f_0 \geq 0$ and that it has no net drift or pressure anisotropy. Since q_{x0} is also affected, we calculate an effective initial ϵ for comparison with the stability theory. Our 1D simulations are run to $t = 24.4 \beta_{e0}/\Omega_{e0}$ and a single 2D simulation is run to $t = 30.6 \beta_{e0}/\Omega_{e0}$.

4. 1D Simulation Results

The 1D simulation, which has an effective $\epsilon = 0.246$, reveals that the heat flux drives waves unstable as predicted by Eq. 3. Magnetic fluctuations perpendicular to \mathbf{B}_0 grow in time (Fig. 2a) and saturate with $\tilde{B}_{sat} \simeq 0.1 B_0$. The waves are right-hand circularly polarized with B_y and B_z 90° out of phase (Fig. 2b). The linear growth rates from the simulation are in good agreement with those obtained from the linear theory (Fig. 1a).

The instability's nonlinear evolution coincides with a surprisingly weak reduction of the total heat flux (Fig. 2a). The reason for this behavior is linked to the mechanism by which whistlers gain energy from particles and are then scattered to reduce the heat flux. In the frame moving with the wave, particles move along concentric circles of constant energy (see Fig. 3d). Resonant electrons moving from high v_\perp to low v_\perp along the constant energy contour in the wave frame lose energy in the simulation frame. If more particles move in this direction than toward higher v_\perp , the waves grow. The portion of the distribution function proportional to ϵ in Eq. 2 and the associated heat flux are shown in Figs. 3a,b. Resonant particles that drive instability have $v_\perp > 1.5$. This picture is confirmed in Fig. 3c, which shows the change in the electron distribution function as a result of the instability. Note the depletion of electrons with high v_\perp and negative v_x . Saturation occurs when this relatively small region is depleted of excess particles. Figure 3b indicates that the bulk heat flux in phase space is carried by $v_x > 0$ particles with high energy, where the distribution function in Fig. 3c is essentially unchanged. Since positive velocity electrons cannot resonate with the 1D whistler instability, significant heat flux suppression cannot occur.

5. 1D Trapping Model

Modest heat flux reduction in 1D is linked to constraints on how electrons are scattered in a collisionless system. In 1D it is only electrons with velocity $v_x = -\Omega/k$ that resonantly drive the instability (Fig. 3c) and we will show that it is only particles close to this resonance that scatter. The substantial number of particles with $v_x > 0$, which carry the bulk of the heat flux (Fig. 3b,c), do not participate in heat flux suppression. The importance of resonant interactions and particle trapping in the scattering of particles by waves in magnetized plasma has been discussed by Karimabadi *et al.*, 1992 based on a formal Hamiltonian theory (Karimabadi *et al.* 1992).

We demonstrate this here by considering electrons in a whistler propagating in the positive x direction, $\tilde{\mathbf{B}} = \tilde{B}(\hat{\mathbf{y}} \sin(kx - \omega t) + \hat{\mathbf{z}} \cos(kx - \omega t))$. In the frame moving with the whistler, the electric field is zero and the energy, $v_x^2 + v_y^2 + v_z^2 = v_0^2$, is conserved (Karimabadi *et al.* 1992). The equation of motion in the wave frame is

$$\frac{d\mathbf{v}}{dt} = -\Omega_e \mathbf{v} \times \hat{\mathbf{x}} - \Omega_e \frac{\mathbf{v} \times \tilde{\mathbf{B}}}{B_0}. \quad (4)$$

The fast time variation of the cyclotron motion can be eliminated by defining the new variables $v_{\pm} = (v_y \pm iv_z)e^{\mp i\Omega_e t}$,

$$\frac{dv_{\pm}}{dt} = v_x \tilde{\Omega}_e e^{\mp i(kx - \omega t)} \quad (5)$$

where $\tilde{\Omega}_e = e\tilde{B}/m_e c$. Shifting to a moving frame with velocity $-\Omega_e/k$, we define $\bar{x} = x + \Omega_e t/k$ with $\bar{v}_x = v_x + \Omega_e/k$ so that Eq. 5 becomes

$$\frac{dv_{\pm}}{dt} = \left(\bar{v}_x - \frac{\Omega_e}{k} \right) \tilde{\Omega}_e e^{\mp ik\bar{x}} \quad (6)$$

with energy conservation now given by $v_+ v_- + (\bar{v}_x - \Omega_e/k)^2 = v_0^2$. The time variation of the particles in this frame is completely controlled by $\tilde{\Omega}_e$. The phase variation of the whistler, however, limits the excursion of v_{\pm} . As v_{\pm} increases or decreases, \bar{v}_x changes due to energy conservation and the wave phase $k\bar{x}$ changes even if \bar{v}_x were initially zero. Consequently, the change in v_{\pm} eventually reverses and the electrons are trapped (Fig. 3d). To show this, we take the time derivative of the energy relation and use Eq. 6 to obtain an equation for $\dot{\bar{v}}_x = \ddot{\bar{x}}$,

$$\ddot{\bar{x}} + \tilde{\Omega} v_{\perp} \cos(k\bar{x} + \phi) = 0, \quad (7)$$

where we have written $v_{\pm} = v_{\perp} e^{\pm i\phi}$. Because trapping limits the excursion of v_{\pm} we can approximate v_{\perp} and ϕ by their initial values $v_{\perp 0}$ and ϕ_0 . The equation for the phase angle

$\theta = k\bar{x} + \phi_0 + \pi/2$ is

$$\ddot{\theta} + \omega_b^2 \sin \theta = 0, \quad (8)$$

where $\omega_b = \sqrt{kv_{\perp 0} \tilde{\Omega}_e}$ is the bounce frequency associated with deeply trapped particles. Integrating once yields

$$\frac{1}{2} \dot{\theta}^2 - \omega_b^2 (1 - \cos \theta) = \frac{1}{2} \dot{\theta}_0^2 \quad (9)$$

where $\dot{\theta}_0$ is the value of $\dot{\theta}$ at $\theta = 0$. The maximum excursion of θ corresponds to the separatrix in the phase space of $\theta - \dot{\theta}$ which is defined by $\dot{\theta}_0 = 0$. Thus, $\Delta\theta = 2\omega_b$ is the trapping width. This corresponds to excursions

$$\frac{\Delta v_x}{v_r} = 2 \sqrt{\frac{v_{\perp 0}}{v_r} \frac{\tilde{B}}{B_0}} \ll 1 \quad (10)$$

in v_x and

$$\frac{\Delta v_{\perp}}{v_r} = 2 \sqrt{\frac{v_r}{v_{\perp 0}} \frac{\tilde{B}}{B_0}} \ll 1 \quad (11)$$

in v_{\perp} , where $v_r = \Omega_e/k$. The same excursion was calculated for ions moving in circularly polarized Alfvén waves (Mace et al. 2012; Dalena et al. 2012). These bounds define the region in velocity space where electrons are scattered. Electrons outside of these ranges, which includes all of the positive velocity particles that carry the bulk of the heat flux, are not scattered.

To confirm the predictions of the trapping theory, we initialize a particle in the frame of a whistler-like wave in 1D with a resonant parallel velocity $v_x = -\Omega_e/k$. The particle trajectory in azimuthal angle $\phi = \arctan(v_{\perp}/v_x)$ in Fig. 3e reveals the trapped bounce motion. The corresponding excursion is shown in Fig. 3d. As predicted, both the frequency and amplitude of oscillations depend on \tilde{B}/B_0 . Particles outside of resonance (not shown) exhibit only small amplitude oscillations.

6. 2D Simulations and Analytic Theory

In contrast with the 1D simulations, the suppression of heat flux in 2D is substantial: for an initial $\epsilon = 0.246$ the heat flux decreases to $\approx 25\%$ of its starting value (Fig. 4a). Perturbations grow at a rate similar to those in the 1D case, have $k\rho_e \sim 1$, and propagate ($\omega/k \simeq v_{Te}/\beta_e$) along and perpendicular to the magnetic field (Fig. 4b) with a characteristic $k_{\perp} = k_y \lesssim k_x$. The saturation time in 2D is only slightly longer than that in 1D. At $t\Omega_e/\beta_e \simeq 12.5$ the amplitude of magnetic perturbations reaches $0.4B_0$. A time sequence

of $\delta f/f_0$ (Fig. 4d-g) shows the development of resonances that were not present in the 1D system. Measured resonant velocities $v_{x,\text{res}}$ are a consequence of $k_\perp \neq 0$ and are given by the condition $\omega - k_x v_x - n\Omega = 0$ where n is any integer (Krall & Trivelpiece 1986; Karimabadi et al. 1992). In particular, we observe that the $n = 1$ ($v_x < 0$), $n = 0$ ($v_x \simeq 0$) and $n = -1$ ($v_x > 0$) resonances all play crucial roles. At the point of saturation f is significantly more isotropic in phase space than f_0 (not shown). Furthermore, the region of concentrated heat flux in Figure 3b ($v_x \gtrsim v_{Te}$) has been drained of excess particles. Whereas in 1D the trapping mechanism was unable to significantly reduce the heat flux, in 2D the availability of the $n = 0$ and $n = -1$ resonances and resonant overlap allow trapping to drive strong pitch-angle scattering over a broad range of velocities. This scattering isotropizes the distribution function by connecting the $v_x < 0$ and $v_x > 0$ regions of phase space.

Trapping equations in the 2D case were derived in Karimabadi et al. (1990) and the results are similar in form to (8) and (9). The results for the $n = 0$ (Landau) and $n = \pm 1$ (Cyclotron) resonances are nearly identical to the 1D case and have the form of Equation 8, where $\omega_b \simeq \sqrt{k v_{\perp 0} \Omega_e}$. To demonstrate the importance of these resonances, we evaluate test particle orbits in the reference frame of a 2D off-angle whistler wave. In this frame the wave takes the form

$$\mathbf{B} = B_0 \hat{\mathbf{x}} + \tilde{B} \left[\left(-\frac{k_y}{k_x} \hat{\mathbf{x}} + \hat{\mathbf{y}} \right) \sin(k_x x + k_y y) + \frac{k}{k_x} \hat{\mathbf{z}} \cos(k_x x + k_y y) \right]$$

where $\tilde{B}_x \neq 0$ and the wave is elliptically, rather than circularly, polarized. In evaluating the particle orbits we take $k_y = k_x$ and consider two different values for \tilde{B}/B_0 : 0.05 and 0.4. Particles are initialized with parallel velocities at the $n = 0, \pm 1$ resonances. In the case of $\tilde{B}/B_0 = 0.05$ we find that trapping widths are small, as predicted by the nonlinear theory (Figure 4c). However, when $\tilde{B}/B_0 = 0.4$, a particle starting at $v_x = \Omega_e/k$ experiences strong trapping and is scattered into the domains of the other two resonances, reversing its original parallel velocity. This is consistent with the results of Karimabadi et al. (1992), in which it was found that resonant overlap occurs when $\delta B/B_0 \simeq 0.3$. It is not a coincidence that saturation takes place once perturbed amplitudes of this size are reached, for it is by this mechanism, in which particles are “handed off” between different resonances, that the particles driving instability are scattered in phase space and wave growth ceases.

7. Conclusions

We have shown using both PIC simulations and linear theory that low-frequency ($\omega \sim \Omega_e/\beta_e$) whistler-like modes in a high- β collisionless plasma are driven unstable by thermal heat flux, even when the pressure is isotropic. The non-linear suppression of the heat flux is negligible in 1D, but becomes substantial in 2D owing to overlapping Landau and cyclotron resonances that lead to effective scattering of electrons. This strong suppression of thermal heat fluxes may be important for understanding the thermodynamics of the ICM in galaxy clusters.

In order to quantify the astrophysical importance of these effects, we calculate an effective conductivity that can be implemented into global, fluid models of the ICM atmosphere. The electron distribution function was earlier calculated by balancing the background temperature gradient with a Krook collision operator, producing the distribution function given in Eq. (2), where the term proportional to $\epsilon = v_{Te}/\nu_{ei}L_T$ describes the heat flux (Levinson & Eichler 1992). Although we have not carried out a scaling study of the rate of wave-driven electron scattering ν_w with parameters, a reasonable hypothesis is that ν_w is given by the peak linear growth rate $\nu_w = \gamma = \epsilon\Omega_e$. Repeating the heat flux calculation by replacing ν_{ei} with ν_w yields $\epsilon = \sqrt{\rho_e/L_T}$ and a heat flux q_{\parallel} given by

$$q_{\parallel} \propto v_{te}nT_e\sqrt{\frac{\rho_e}{L_T}}. \quad (12)$$

This is reduced from the collisionless, free-streaming value by the factor $\sqrt{\rho_e/L_T}$, which can be as small as 10^{-6} for the ICM.

A caveat is that our numerical models are run with large heat fluxes ($\epsilon \approx 0.25$) whereas typical heat fluxes in the ICM can be much smaller. While linear theory shows that the whistler instability exists for any non-zero heat flux, it is possible that there exists a threshold heat flux below which whistler-mediated scattering of electrons is ineffective. On the other hand, our present simulations are initial value problems that relax to an equilibrium system in a periodic box, while a more realistic configuration would continually drive a heat flux down a temperature gradient, explicitly linking heat flux and temperature gradient. The unlimited supply of free energy into the system would likely drive the large-amplitude perturbations that satisfy the resonance overlap condition, $\delta B/B_0 \gtrsim 0.3$, regardless of how small the driving heat flux is. This will likely lead to a saturated state in which injection and disruption of heat flux balance and so differ significantly from that of the initial value problem in which heat flux relaxes to a low level. Whistler turbulence from the heat flux instability might also be damped or driven unstable by electron pressure

anisotropies in the ICM and may couple to ion-scale anisotropy-driven modes. These issues will be explored in future work.

The authors wish to acknowledge NSF grant AST1333514 and NASA/SAO Chandra Theory grant TM617008X, and M.W. Kunz for helpful discussion.

REFERENCES

- Binney, J., & Cowie, L. L. 1981, *ApJ*, 247, 464
- Churazov, E., Forman, W., Jones, C., & Böhringer, H. 2000, *A&A*, 356, 788
- Churazov, E., Sunyaev, R., Forman, W., & Böhringer, H. 2002, *MNRAS*, 332, 729
- Croton, D. J., Springel, V., White, S. D. M., De Lucia, G., Frenk, C. S., et al. 2006, *MNRAS*, 365, 11
- Dalena, S., Greco, A., Rappazzo, A. F., Mace, R. L., & Matthaeus, W. H. 2012, *Phys. Rev. E*, 86
- Fabian, A. C. 1994, *ARA&A*, 32, 277
- Fabian, A. C., Reynolds, C. S., Taylor, G. B., & Dunn, R. J. H. 2005, *MNRAS*, 363, 891
- Gary, S. P., & Li, H. 2000, *ApJ*, 529, 1131
- Karimabadi, H., Akimoto, K., Omidi, N., & Menyuk, C. R. 1990, *Physics of Fluids B*, 2, 606
- Karimabadi, H., Krauss-Varban, D., & Terasawa, T. 1992, *J. Geophys. Res.*, 97, 13,853
- Komarov, S. V., Churazov, E. M., Kunz, M. W., & Schekochihin, A. A., 2016, *MNRAS*, 460, 467
- Krall, N. A., & Trivelpiece, A. W. 1986, *Principles of Plasma Physics* (San Francisco Press, Inc.), 368–441
- Kunz, M. W., Schekochihin, A. A., & Stone, J. M. 2014, *Physical Review Letters*, 112, 205003
- Levinson, A., & Eichler, D. 1992, *ApJ*, 387, 212

- Li, T. C., Drake, J. F., & Swisdak, M. 2012, *Ap. J.*, 757
- Mace, R. L., Dalena, S., & Matthaeus, W. H. 2012, *Phys. Plasmas*, 19
- Ramani, A., & Laval, G. 1978, *Physics of Fluids*, 21, 980
- Reynolds, C. S., Heinz, S., & Begelman, M. C. 2002, *MNRAS*, 332, 271
- Rincon, F., Schekochihin, A. A., & Cowley, S. C. 2015, *MNRAS*, 447, L45
- Riquelme, M., Quataert, E., & Verscharen, D. 2016, *ArXiv e-prints*
- Spitzer, L. 1956, *Physics of Fully Ionized Gases* (New York: Interscience)
- Yang, H.-Y. K., & Reynolds, C. S. 2016, *ApJ*, 818, 181
- Zeiler, A., Biskamp, D., Drake, J. F., Rogers, B. N., Shay, M. A., & Scholer, M. 2002, *J. Geophys. Res.*, 107, 1230

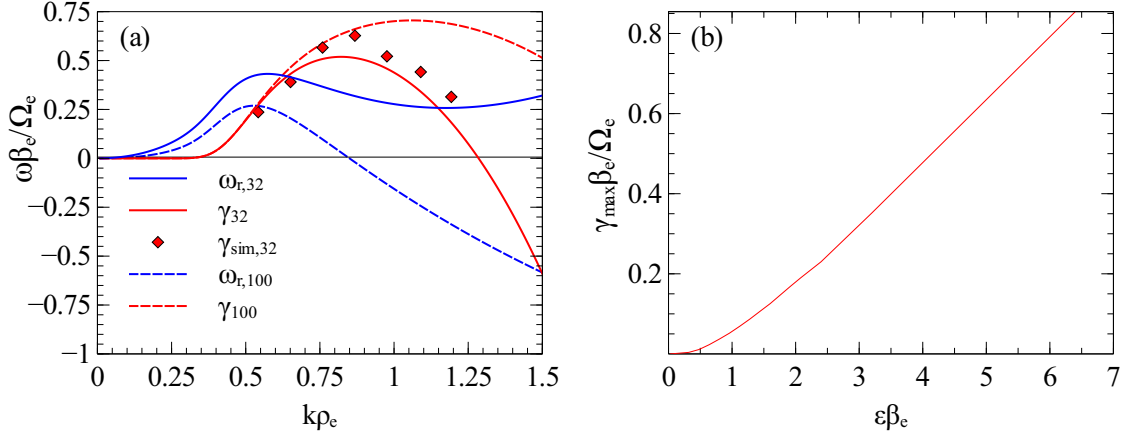


Fig. 1.— Analytic dispersion relation of the heat-flux-driven whistler-like wave in a plasma with $\beta_e = 32$ (solid lines), 100 (dashed lines) and $\epsilon = 0.133$. (a) Real frequency (blue) and growth rate (red) of the instability as calculated from Eq. (3). The red diamonds show growth rates at discrete values of k taken from a 1D simulation with the same ϵ and $\beta = 32$. (b) Growth rate of the maximally growing mode for a range of $\epsilon\beta$.

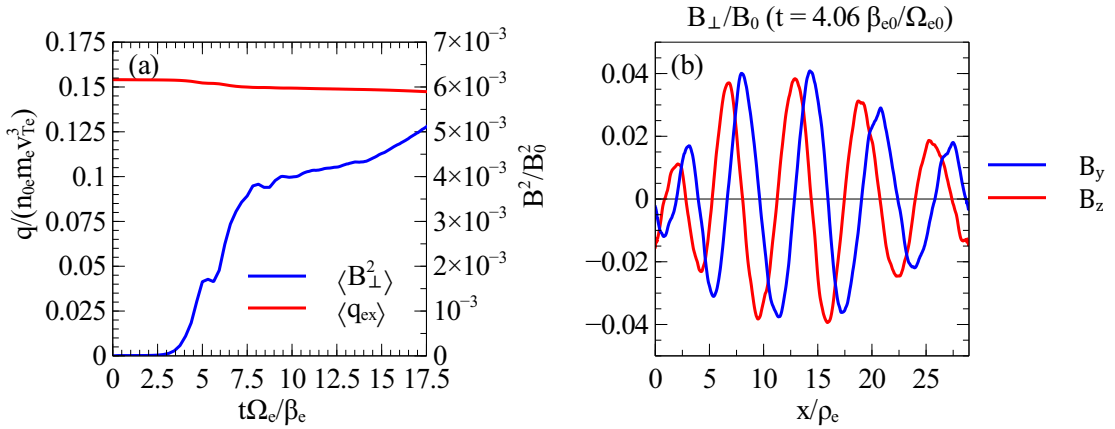


Fig. 2.— 1D PIC Simulation Results. (a) Average heat flux and mean squared value of the perturbed magnetic field. (b) Whistler-like phase relation between B_y and B_z .

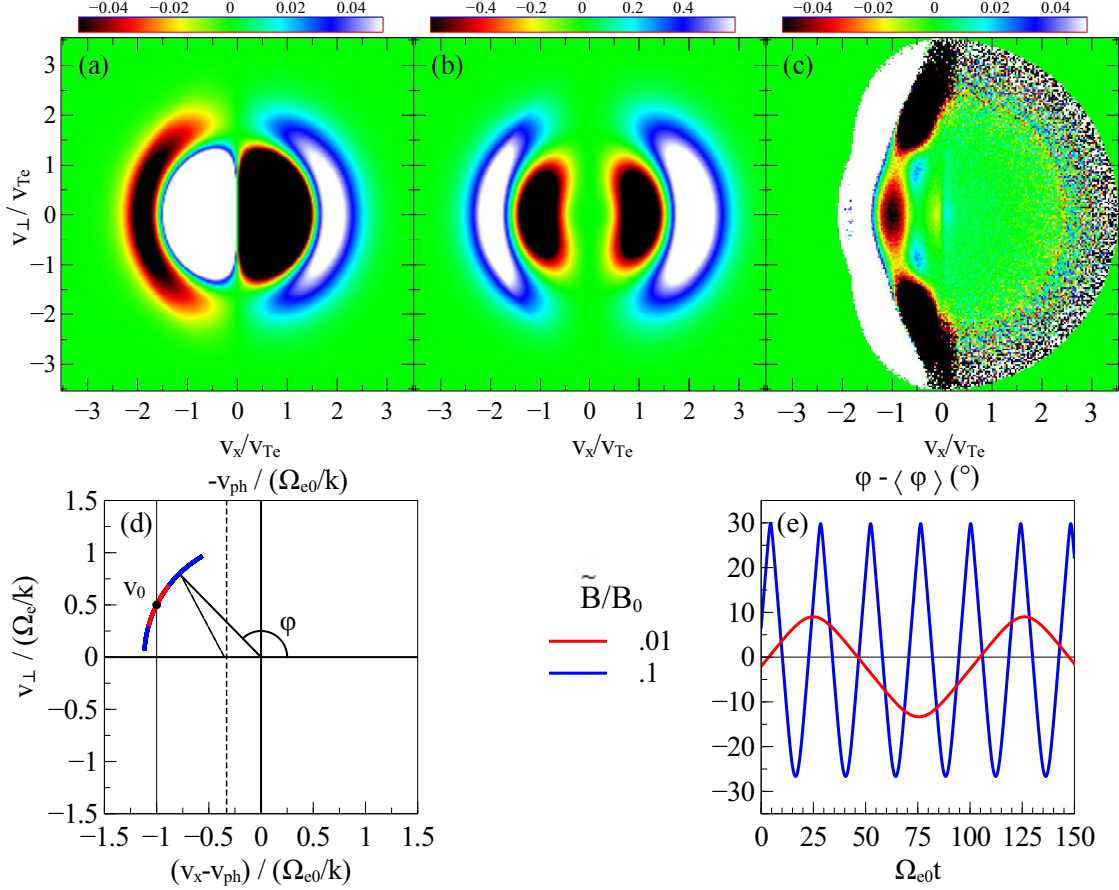


Fig. 3.— Phase space plots and particle trapping in 1D. (a) $(f_0 - f_M)/\max(f_0 - f_M)$ from the PIC simulation. (b) The local heat flux, $(f_0 - f_M)v^2v_x/\max[(f_0 - f_M)v^2v_x]$. (c) $\delta f/f_0 = (f - f_0)/f_0$ from the PIC simulation at late time, $t = 9.34 \beta_{e0}/\Omega_{e0}$. (d) Trajectories of trapped test particles in the wave frame of the 1D whistler for small (red) and large (blue) \tilde{B} . The initial parallel velocity is the resonant velocity $-\Omega/k$. The lab frame is marked with the dashed lines. In (e) temporal evolution of the angle $\phi = \arctan(v_\perp/v_x)$ for the test particles in (d).

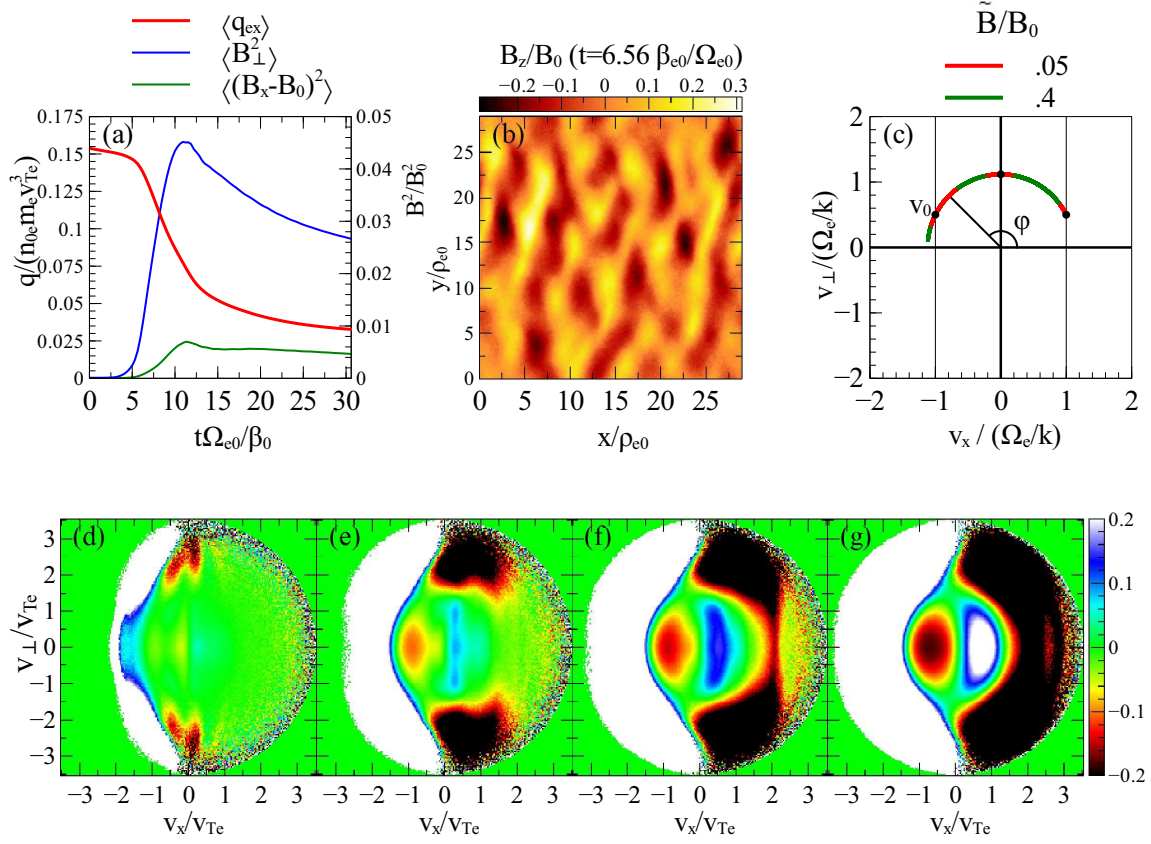


Fig. 4.— 2D simulation results and trapping theory. (a) Averages of the heat flux and mean-squared values of the perturbed perpendicular and parallel magnetic fields versus time. (b) The 2-dimensional structure of the magnetic field B_z . (c) In the wave frame of a 2D whistler, the orbits of trapped test particles for two values of \tilde{B} . The $v_x - v_{\perp}$ phase space of $\delta f/f_0 = (f - f_0)/f_0$ at $t\Omega_{e0}/\beta_{e0} = 5.31$ (d), 8.12 (e), 10.94 (f), and 30.6 (g).